

Echoes and quasi-normal modes of perturbations around Schwarzschild traversable wormholes

Hao Yang^{1,*}, Zhong-Wu Xia^{1,†}, and Yan-Gang Miao^{1,2,‡}

¹*School of Physics, Nankai University, Weijin Road 94, Tianjin 300071, China*

²*Faculty of Physics, University of Vienna, Boltzmannngasse 5, A-1090 Vienna, Austria*

Abstract

We investigate the waveforms and quasi-normal modes around Schwarzschild traversable wormholes under different field perturbations, including the scalar field perturbation, the electromagnetic (vector) field perturbation and the gravitational (tensor) field perturbation. By comparing Schwarzschild traversable wormholes with Schwarzschild black holes, we find some unique properties for the former. At first, the perturbation waveform includes echoes and damping oscillations around Schwarzschild traversable wormholes, while it has only the damping waveform around Schwarzschild black holes. Secondly, the difference between adjacent peaks of echoes varies with the mass parameter and the defect parameter in the waveform around Schwarzschild traversable wormholes, while it always keeps constant around Schwarzschild black holes. Thirdly, the ordinary isospectrality between the odd and even parities no longer exists in the quasi-normal modes of gravitational perturbations around Schwarzschild traversable wormholes, but an alternative isospectrality appears. According to these properties, we summarize a scenario for estimating the mass parameter and the defect parameter of Schwarzschild traversable wormholes through the waveforms and quasi-normal modes. Our analyses provide a more profound comprehension of the inherent characteristics of Schwarzschild traversable wormholes.

*E-mail address: hyang@mail.nankai.edu.cn

†E-mail address: 2120210160@mail.nankai.edu.cn

‡Corresponding author. E-mail address: miaoyg@nankai.edu.cn

Contents

1	Introduction	3
2	Schwarzschild traversable wormholes	4
3	Perturbation equation and finite difference method	5
3.1	Perturbation equation	5
3.2	Finite difference method	7
4	Scalar field perturbation	8
4.1	Echo waveform	8
4.2	Damping oscillation	11
4.3	Scenario for fixing parameters	13
5	Electromagnetic field perturbation	14
5.1	Echo waveform	15
5.2	Damping oscillation	16
6	Gravitational field perturbation	17
6.1	Echo waveform	17
6.2	Damping oscillation and isospectrality	19
7	Conclusion and discussion	24

1 Introduction

A wormhole is a spacetime structure that connects two regions in our universe or in a multiverse. The introduction of wormholes can be traced back to almost 100 years ago and the originally constructed wormholes are untraversable [1, 2] owing to their instability and tidal gravitational forces, etc. And traversable wormholes were proposed [3, 4] in 1980s. Soon later, a general method to construct traversable wormholes, called the “cut and paste” technique, was suggested [5–7], whose core idea is to connect two identical template spacetimes with a common hypersurface. Nowadays, this method has widely been used [8–19] in the construction of traversable wormholes under various theories. However, so far, traversable wormholes are still in the stage of theoretical conceptions and have not been verified by experiments.

At present, it gradually becomes feasible to verify gravitational theories from observations after the continuous development of gravitational wave detection technology [20–22]. Moreover, the difference of spacetime structures between a wormhole (constructed by the “cut and paste” technique) and a template spacetime is also expected [23–26] to be distinguished by observations. In the present work we start with a Schwarzschild traversable wormhole that comes [5] from a Schwarzschild spacetime as a template. Then we try to investigate the difference of spacetime structures between a Schwarzschild traversable wormhole and a Schwarzschild black hole because this difference is probably hidden in alterations of some observables, such as echoes and quasi-normal modes.

According to the perturbation theory of spacetime [27, 28], we know that a perturbation waveform is generated in a perturbed spacetime. The perturbation waveform is typically a damping oscillation, meaning that its amplitude gradually decreases over time when it oscillates periodically. It is usually called a quasi-normal mode whose characteristic frequency can be written as

$$\omega = \omega_{\text{R}} + i\omega_{\text{I}}, \quad (1)$$

where ω_{R} denotes the oscillation frequency and ω_{I} the decay rate. We note that the oscillation frequency presents the intrinsic properties of spacetimes (black holes or traversable wormholes) and thus it is fixed by the parameters of metrics. When a spacetime structure changes from a black hole to a traversable wormhole, its corresponding quasi-normal modes alter [29] accordingly, providing us the possibility to judge the existence of traversable wormholes. In addition, the perturbation waveform is probably an echo [30–33] in a wormhole spacetime. At this time, the waveform exhibits periodic pulse-shaped enhancements, which is absent in Schwarzschild black holes. Based on the types of waveforms, we can perform the judgment for the existence of traversable wormholes. To this end, we analyze the difference between Schwarzschild traversable wormholes and Schwarzschild black holes from the perspectives of perturbation waveforms and quasi-normal modes.

The paper is organized as follows. In Sec. 2, we make a detailed analysis to Schwarzschild traversable wormholes. In Sec. 3, we give perturbation equations under different field perturbations and introduce the finite difference method. In Sec. 4, we analyze the waveforms and quasi-normal modes under scalar field perturbations and propose a scenario to estimate the parameters of Schwarzschild traversable wormholes. In Sec. 5, we further investigate the waveforms and quasi-normal modes under electromagnetic field perturbations. In Sec. 6, we check the isospectrality of odd and even parities in gravitational perturbations for Schwarzschild traversable wormholes. Finally, we give our conclusion and discussion in Sec. 7.

2 Schwarzschild traversable wormholes

Schwarzschild traversable wormholes are constructed [5] by the ‘‘cut and paste’’ technique together with the Schwarzschild spacetime serving as a template. The main steps are briefly introduced as follows. At first, we consider the Schwarzschild spacetime described by the metric,

$$ds^2 = - \left(1 - \frac{2M}{\chi}\right) dt^2 + \left(1 - \frac{2M}{\chi}\right)^{-1} d\chi^2 + \chi^2 (d\theta^2 + \sin^2 \theta d\phi^2), \quad (2)$$

where M is the mass, χ the radial coordinate, $\chi \in [0, +\infty)$, and the horizon is located at $\chi = 2M$. Then, we take two copies of this manifold, labeled with ‘‘1’’ and ‘‘2’’, respectively, and dig out two four-dimensional regions, $\Omega_i \equiv \{\chi_i < b | b > 2M\}$, $i = 1, 2$, in the two copied manifolds, where b is a constant and is taken to be $b > 2M$ in order to ensure that there are no horizons in the remaining spacetimes. Now each manifold is a geodesically incomplete manifold with a timelike hypersurface boundary, $\partial\Omega_i \equiv \{\chi_i = b | b > 2M\}$, $i = 1, 2$. Finally, we combine these two manifolds by taking $\partial\Omega_1 = \partial\Omega_2 \equiv \partial\Omega$ and obtain a geodesically complete wormhole manifold with the throat at $\partial\Omega$.

The above process can be implemented when we make the transformation $\chi \rightarrow \chi(r)$ in Eq. (2) and obtain the corresponding metric,

$$ds^2 = - \left[1 - \frac{2M}{\chi(r)}\right] dt^2 + \left[1 - \frac{2M}{\chi(r)}\right]^{-1} \chi'^2(r) dr^2 + \chi^2(r) (d\theta^2 + \sin^2 \theta d\phi^2). \quad (3)$$

where r is regarded as a parameter, $r \in (-\infty, +\infty)$, and $\chi(r)$ satisfies the following three conditions:

- $\chi(r)$ is an even function in order to ensure that the metric with $r < 0$ is a copy to that with $r > 0$ and both of them are copies of a Schwarzschild spacetime.
- $d\chi(r)/dr$ is always greater than zero when $r > 0$, so as to ensure that $\chi(r)$ and r are one-to-one correspondence.
- $\chi(0) = a$, which means that we remove the region $\chi < a$ from a Schwarzschild spacetime and connect two identical spacetimes¹ at $r = 0$.

One previous option [34, 35], for instance, was $\chi(r) = \sqrt{r^2 + a^2}$. However, our following discussions do not depend on $\chi(r)$, so we do not give its specific form. Meanwhile, we do not assume $a > 2M$ because we want to analyze how the event horizon affects the observations of wormholes. The spacetime described by Eq. (3) has the following three structures depending on the value of a :

- When $0 < a < 2M$, there exists a horizon, $\chi = 2M$, and Eq. (3) describes a black hole. In this situation, the wormhole throat located at $\chi = a$ is hidden by the horizon. However, there is no distinction between this solution and a Schwarzschild black hole outside the event horizon. Since the region within the event horizon cannot be observed from outside, we are not able to determine whether the traversable wormhole exists or not.

¹Here the spacetime means the remaining one after a Schwarzschild spacetime is dug out by the four-dimensional region, $\Omega \equiv \{\chi < b | b > 2M\}$.

- When $a = 2M$, the coordinate speed of light vanishes at $r = 0$, i.e., $\frac{d\chi(r)}{dt}\big|_{r=0} = 0$, where we choose $\chi(r)$ as the radial coordinate since it represents the area radius in the spacetime. At this time, the solution is not a black hole, but a one-way wormhole with a null-like throat located at $\chi = 2M$. However, considering the similarity between the null-like throat and the event horizon, we are still not able to determine whether the traversable wormhole exists or not.
- When $a > 2M$, no horizons exist and $\frac{d\chi(r)}{dt} \neq 0$ in the region of $r \in (-\infty, +\infty)$. Eq. (3) describes [36] a traversable wormhole whose throat is located at $\chi(0) = a$, where negative values of r represent a geometric universe on the opposite side of the observer's own universe. In this situation, the “cut and paste” technique works, which will be confirmed by distinguishing a traversable wormhole from a black hole. Such changes of spacetime structures will be analyzed by the alterations of observables, e.g., echoes and quasi-normal modes.

3 Perturbation equation and finite difference method

3.1 Perturbation equation

Generally, three types of fields are used to perturb [28] a spacetime, which are the scalar field perturbation, the electromagnetic (vector) field perturbation, and the gravitational (tensor) field perturbation. The wave function Φ_s of the three perturbation fields satisfies [28, 37] the following Schrödinger-like equation,

$$\frac{d^2\Phi_s}{dr_*^2} - \frac{d^2\Phi_s}{dt^2} - V_s\Phi_s = 0, \quad (4)$$

where V_s stands for effective potential, s spin with $s = 0, 1, 2$ for scalar, vector, and tensor perturbation fields, respectively, and r_* turtle coordinate defined by

$$dr_* \equiv \frac{\chi(r)}{\chi(r) - 2M} |\chi'(r)| dr. \quad (5)$$

We solve the differential equation for black holes and traversable wormholes, respectively.

- Solving Eq. (5) for a black hole with horizons, we obtain

$$r_* = \chi(r) + 2M \ln \left(\frac{\chi(r)}{2M} - 1 \right), \quad (6)$$

where its lower boundary is located at the outer horizon, $\chi(r) = 2M$, and its upper boundary is located at infinity, $\chi(r) = +\infty$, i.e., the turtle coordinate takes the range, $r_* \in (-\infty, +\infty)$. In other words, the boundaries of equations of motion are determined by the outer event horizon and the infinity of the observer's universe.

- Solving Eq. (5) for a Schwarzschild traversable wormhole without horizons and singularities, we

obtain

$$r_* = \begin{cases} 2a + 4M \ln \left(\frac{a}{2M} - 1 \right) - \chi(r) - 2M \ln \left(\frac{\chi(r)}{2M} - 1 \right), & r < 0, \\ \chi(r) + 2M \ln \left(\frac{\chi(r)}{2M} - 1 \right), & r \geq 0, \end{cases} \quad (7)$$

where the range of r_* is still $(-\infty, +\infty)$, but the wormhole's lower bound is at $\chi(r) = +\infty$ with $r < 0$ and upper bound is at $\chi(r) = +\infty$ with $r > 0$. This shows that the boundaries of equations of motion are determined by the infinity of observer's opposite universe and the infinity of observer's own universe, where the two universes are connected through traversable wormholes. And the throat of traversable wormholes is located at $r_* = a + 2M \ln \left(\frac{a}{2M} - 1 \right)$.

The effective potential of scalar field perturbations reads [28]

$$V_{s=0} = \left(1 - \frac{2M}{\chi(r)} \right) \left[\frac{l(l+1)}{\chi(r)^2} + \frac{2M}{\chi(r)^3} \right], \quad (8)$$

where l is azimuthal number and it satisfies $l \geq |s|$. The effective potential of electromagnetic field perturbations takes [28] the form,

$$V_{s=1} = \left(1 - \frac{2M}{\chi(r)} \right) \left[\frac{l(l+1)}{\chi^2(r)} \right]. \quad (9)$$

Gravitational field perturbations are divided into odd parity ones and even parity ones, where the parity equals $(-1)^{l+1}$ for the former and $(-1)^l$ for the latter under the transformation of $\theta \rightarrow -\theta$, respectively. The wave function of odd parity perturbations is called [38] the Regge-Wheeler function, $\Phi_{s=2}^-$, and its corresponding effective potential is

$$V_{s=2}^- = \left(1 - \frac{2M}{\chi(r)} \right) \left[\frac{l(l+1)}{\chi^2(r)} - \frac{6M}{\chi^3(r)} \right]. \quad (10)$$

Moreover, the wave function of even parity perturbations is called [39] the Zerilli function, $\Phi_{s=2}^+$, and its corresponding effective potential is

$$V_{s=2}^+ = 2 \left(1 - \frac{2M}{\chi(r)} \right) \frac{9M^3 + 3\lambda^2 M \chi^2(r) + \lambda^2(1+\lambda)\chi^3(r) + 9M^2 \lambda \chi(r)}{\chi^3(r)(3M + \lambda \chi(r))^2}, \quad (11)$$

where $\lambda = (l-1)(l+2)/2$. Considering $l \geq |s|$, we take $l = 2$ in our following calculations, which is valid for the three field perturbations. In addition, we note that our subsequent discussions will not depend on specific forms of $\chi(r)$ because Eqs. (4) and (6)-(11) do not contain r explicitly.

For the sake of generality, we adopt dimensionless quantities defined as follows:

$$\bar{\chi}(r) \equiv \frac{\chi(r)}{2M}, \quad \bar{t} \equiv \frac{t}{2M}, \quad \bar{a} \equiv \frac{a}{2M}, \quad \bar{V}_s \equiv 4M^2 V_s, \quad \bar{r}_* \equiv \frac{r_*}{2M}. \quad (12)$$

After using the above dimensionless quantities, we rewrite Eqs. (4) and (6)-(11) as follows:

$$\frac{d^2 \Phi_s}{d\bar{r}_*^2} - \frac{d^2 \Phi_s}{d\bar{t}^2} - \bar{V}_s \Phi_s = 0, \quad (13)$$

where the turtle coordinate takes the forms,

$$\bar{r}_* = \bar{\chi}(r) + \ln(\bar{\chi}(r) - 1), \quad (14)$$

and

$$\bar{r}_* = \begin{cases} 2\bar{a} + 2 \ln(\bar{a} - 1) - \bar{\chi}(r) - \ln(\bar{\chi}(r) - 1), & r < 0, \\ \bar{\chi}(r) + \ln(\bar{\chi}(r) - 1), & r \geq 0, \end{cases} \quad (15)$$

for black holes and traversable wormholes, respectively, and the effective potentials of different field perturbations read

$$\bar{V}_{s=0} = \left(1 - \frac{1}{\bar{\chi}(r)}\right) \left[\frac{l(l+1)}{\bar{\chi}^2(r)} + \frac{1}{\bar{\chi}^3(r)} \right], \quad (16)$$

$$\bar{V}_{s=1} = \left(1 - \frac{1}{\bar{\chi}(r)}\right) \left[\frac{l(l+1)}{\bar{\chi}^2(r)} \right], \quad (17)$$

$$\bar{V}_{s=2}^- = \left(1 - \frac{1}{\bar{\chi}(r)}\right) \left[\frac{l(l+1)}{\bar{\chi}^2(r)} - \frac{3}{\bar{\chi}^3(r)} \right], \quad (18)$$

$$\bar{V}_{s=2}^+ = \left(1 - \frac{1}{\bar{\chi}(r)}\right) \frac{9 + 12\lambda^2\bar{\chi}^2(r) + 8\lambda^2(1+\lambda)\bar{\chi}^3(r) + 18\lambda\bar{\chi}(r)}{\bar{\chi}^3(r)(3 + 2\lambda\bar{\chi}(r))^2}. \quad (19)$$

We note that Eqs. (13)-(15) do not explicitly contain M , which means that the dimensionless treatment changes a double-parameter issue related to M and a into a single-parameter one related only to \bar{a} . This feature will greatly simplify our subsequent calculations and give the results with generality.

3.2 Finite difference method

When a spacetime structure changes, such as from a black hole to a traversable wormhole, the perturbation equation that associates with the spacetime structure will be varying accordingly, which inevitably alters the time-domain behavior of perturbations. Here we employ the finite difference method [30, 32] and the Prony method [37, 40] to calculate perturbation waveforms and quasi-normal modes. We start with discretizing the coordinate space (\bar{t}, \bar{r}_*) , so that $\Phi_s(\bar{t}, \bar{r}_*)$ becomes $\Phi_s(j\Delta\bar{t}, k\Delta\bar{r}_*)$, where j and k are integers, and $\Delta\bar{t}$ and $\Delta\bar{r}_*$ are step sizes of coordinates. For the sake of convenience, we write $\Phi_s(j\Delta\bar{t}, k\Delta\bar{r}_*)$ and $\bar{V}_s(k\Delta\bar{r}_*)$ as $\Phi_s(j, k)$ and $\bar{V}_s(k)$, respectively. As long as the step sizes are small enough, we can change the differential equation, Eq. (13), into the following difference equation:

$$\begin{aligned} & -\frac{\Phi_s(j+1, k) - 2\Phi_s(j, k) + \Phi_s(j-1, k)}{\Delta\bar{t}^2} + \frac{\Phi_s(j, k+1) - 2\Phi_s(j, k) + \Phi_s(j, k-1)}{\Delta\bar{r}_*^2} \\ & - \bar{V}_s(k)\Phi_s(j, k) = 0, \end{aligned} \quad (20)$$

from which we obtain the iterative formula of Φ_s ,

$$\Phi_s(j+1, k) = -\Phi_s(j-1, k) + \left[2 - 2\frac{\Delta\bar{t}^2}{\Delta\bar{r}_*^2} - \Delta\bar{t}^2\bar{V}_s(k) \right] \Phi_s(j, k) + \frac{\Delta\bar{t}^2}{\Delta\bar{r}_*^2} [\Phi_s(j, k+1) + \Phi_s(j, k-1)]. \quad (21)$$

In terms of this iterative formula, we can compute numerically perturbation waveforms and quasi-normal modes, i.e., wave functions and quasi-normal mode frequencies. Here the corresponding boundary conditions are ingoing waves in $\bar{r}_* \rightarrow -\infty$ and outgoing waves in $\bar{r}_* \rightarrow \infty$. In subsequent calculations, we take the initial wave packet as a Gaussian wave packet and the initial condition as

$$\Phi_s(\bar{t} = 0, \bar{r}_*) = e^{-\frac{(\bar{r}_* - A)^2}{2B^2}}, \quad \Phi_s(\bar{t} < 0, \bar{r}_*) = 0, \quad (22)$$

where A is the center of Gaussian packets, and B the width. In the present work, $B = 1$ is set and the value of A is chosen accordingly. Moreover, considering the von Neumann stability condition [41],

$$\frac{\Delta \bar{t}}{\Delta \bar{r}_*} < 1, \quad (23)$$

we take $\Delta \bar{t} / \Delta \bar{r}_* = 0.25$. According to the relationship [28, 37, 42] between wave functions $\Phi_s(\bar{t})$ and frequencies ω_j of quasi-normal modes,

$$\Phi_s(\bar{t}) \simeq \sum_{j=1}^p C_j e^{-i2M\omega_j \bar{t}}, \quad (24)$$

where C_j 's are excitation coefficients of p main quasi-normal modes, we extract p main modes from $\Phi_s(\bar{t})$ by using the Prony method [37, 40] in the following three sections for the scalar, vector, and tensor field perturbations, respectively. Among these p quasi-normal modes, the dominant one that has the largest $|C_j|$ provides the most contributions to waveforms.

4 Scalar field perturbation

In this section we give the result that the waveform of scalar field perturbations contains two types, where one type includes both the echo and damping oscillation around Schwarzschild traversable wormholes, while the other type includes only the damping oscillation around Schwarzschild black holes.

4.1 Echo waveform

When $\bar{a} > 1$ and $\bar{a} - 1 \ll 1$, the perturbation waveform around Schwarzschild traversable wormholes takes an echo waveform, i.e., the waveform exhibits periodic pulse-shaped enhancements. In this situation, the position of the throat, $\bar{\chi} = \bar{a}$, is very close to the event horizon of Schwarzschild black holes, $\bar{\chi} = 1$, indicating that the Schwarzschild traversable wormhole has just evolved from a Schwarzschild black hole or is about to transform into it.

The generation of echoes is closely related to the shape of effective potentials under scalar field perturbations. The effective potentials for a varying \bar{a} , see Eq. (16) which results in the presence of echo waveforms, are depicted by Fig. 1, showing that each of the four effective potentials exhibits two barriers, the left barrier and the right one, where the four left barriers are separated but the four right ones are overlapped under different values of the parameter \bar{a} . The reason for this phenomenon is that the Schwarzschild traversable wormhole is formed when the Schwarzschild spacetime as a template is

cut off at the throat ($\bar{\chi} = \bar{a}$) and then the “mirror world” of the remaining spacetime is glued. In other words, the effective potential of Schwarzschild traversable wormholes consists of two parts, the first part is the effective potential of the Schwarzschild spacetime cut off at the throat and the second part is the mirror of the first part, i.e., the first part is mapped to the range of $r < 0$. Since the effective potential of the Schwarzschild spacetime is independent of the parameter \bar{a} , its potential barrier does not change with \bar{a} and appears an overlapping potential barrier under different \bar{a} , see the rightmost barrier in Fig. 1. The symmetry axis of effective potentials corresponds to the position of the throat of Schwarzschild traversable wormholes, namely, $\bar{r}_* = \bar{a} + \ln(\bar{a} - 1)$. Fig. 1 illustrates that echoes can only be generated in a double-barrier potential with a sufficiently large interval between the two peaks of barriers, and such an interval acts as a resonant cavity.

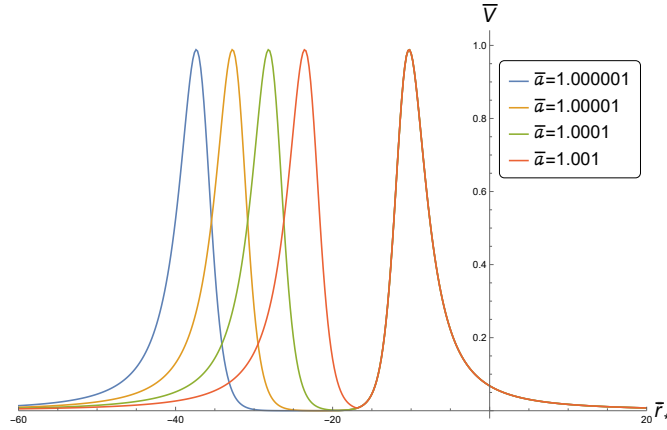


Figure 1: The effective potentials that result in the presence of echo waveforms under the scalar field perturbation with $l = 2$. The blue, orange, green, and red curves correspond to $\bar{a} = 1.000001, 1.00001, 1.0001, \text{ and } 1.001$, respectively. The right barriers of these four curves are overlapped.

By using the finite difference method and the Prony method introduced in Sec. 3.2, we draw up the echo waveforms around Schwarzschild traversable wormholes in Fig. 2 for different values of the parameter \bar{a} , and we also give the time that the first three echoes occur and the peaks of these echoes in Table 1 under different values of the parameter \bar{a} . We conclude that the echo waveforms around Schwarzschild traversable wormholes have the following characteristics:

- For a fixed parameter \bar{a} , the three echoes appear intermittently, and their peaks from the first to third ones gradually decrease owing to wave scattering by the potential barriers during propagation.
- Under different values of the parameter \bar{a} , the peaks of echoes are almost equal because the peaks of potential barriers are exactly the same.
- When the parameter \bar{a} increases, the time that each echo occurs becomes short and the time interval between adjacent-echoes also becomes short because the distance between the two potential barriers is decreasing.

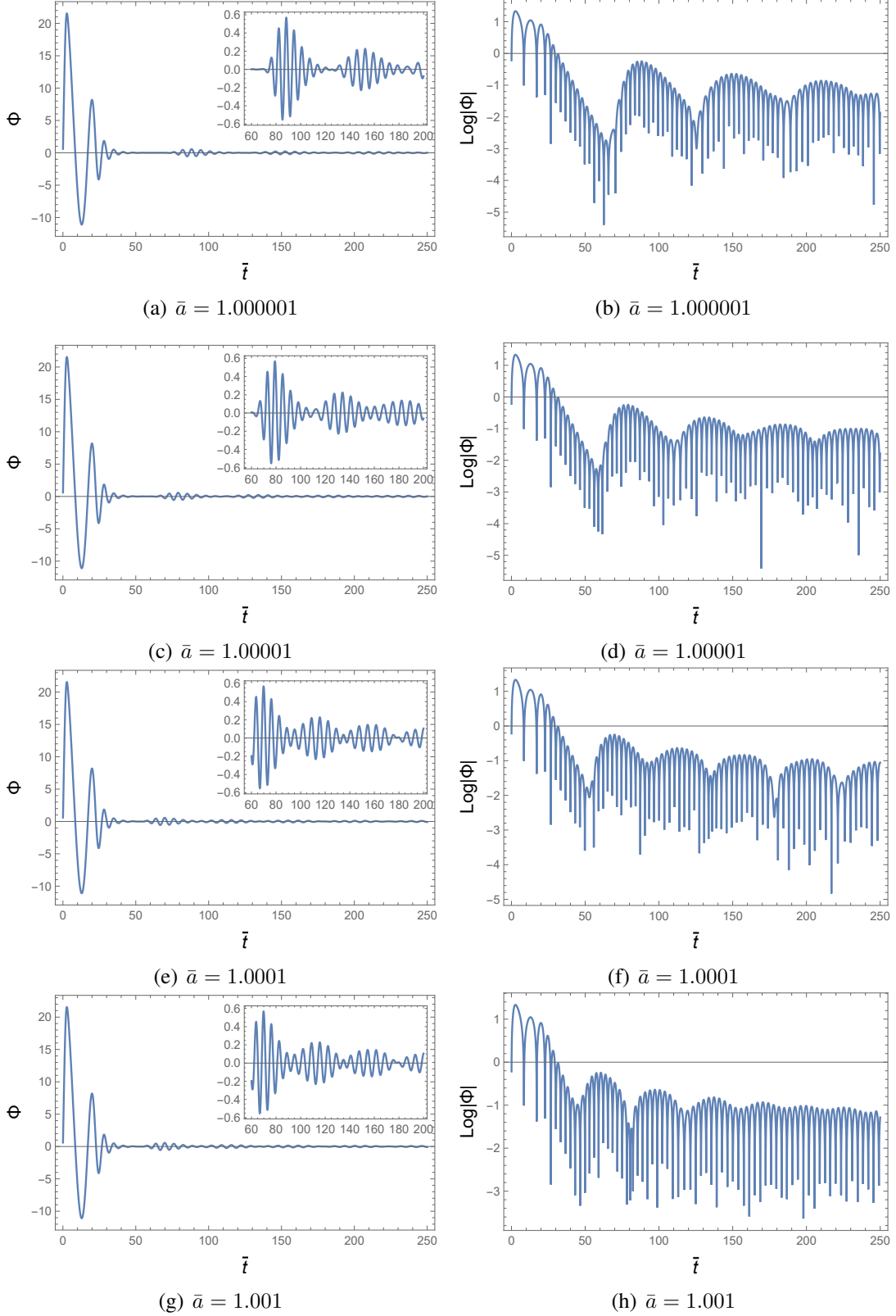


Figure 2: The echo waveforms around Schwarzschild traversable wormholes for different values of the parameter \bar{a} under the scalar field perturbation with $l = 2$. The left diagrams show how the wave function Φ varies with the time \bar{t} , and the right ones show how the function $\log |\Phi|$ varies with the time \bar{t} .

Table 1: The time that the first three echoes occur and the peaks of these echoes under different values of the parameter \bar{a} for scalar field perturbations.

\bar{a}	Echo 1 (T)	Echo 1 (P)	Echo 2 (T)	Echo 2 (P)	Echo 3 (T)	Echo 3 (P)
1.000001	88.30	0.567498	149.20	0.228950	209.90	0.138538
1.00001	79.10	0.567204	130.75	0.227911	182.20	0.136524
1.0001	69.85	0.566514	112.25	0.231643	158.00	0.146416
1.001	60.65	0.568974	97.25	0.228812	137.35	0.152663

In summary, when a Schwarzschild traversable wormhole has just evolved from a Schwarzschild black hole or is about to transform into a Schwarzschild black hole, the scalar field perturbation generates an echo waveform in the wormhole spacetime. According to Eqs. (15) and (16), the effective potential barrier at $\bar{r}_*(r > 0)$ does not change with \bar{a} . When \bar{a} increases, the position of the wormhole's throat, i.e. $\bar{r}_*|_{r=0} = \bar{a} + \ln(\bar{a} - 1)$, increases, resulting in a decrease in the distance between the throat and the effective potential barrier at $\bar{r}_*(r > 0)$. Since the two potential barriers are symmetric to the wormhole throat, the increase in \bar{a} will reduce the interval between the effective potential barrier at $\bar{r}_*(r > 0)$ and its mirror barrier at $\bar{r}_*(r < 0)$. Therefore, the echoes occur more frequently for a bigger \bar{a} . As known, however, the scalar field perturbation only produces a damped oscillation waveform without echoes in the case of Schwarzschild black holes.

4.2 Damping oscillation

As \bar{a} is going to large, the perturbation waveform gradually changes from echoes to damping oscillations. Here we start our analysis from $\bar{a} \geq 1.1$, where only the damping oscillation waveform exists in the spacetime. The characteristic frequency of damping oscillations is described by quasi-normal modes, which consists of a real part and an imaginary part. Here we again use the finite difference method and the Prony method introduced in Sec. 3.2 to calculate the waveform and quasi-normal modes in the parameter range of $\bar{a} \geq 1.1$. The dominant quasi-normal modes are given in Table 2, where the data are dimensionless because the frequency ω has been multiplied by the factor $2M$, and the relation between the logarithm wave function $\log |\Phi|$ and the dimensionless time \bar{t} is depicted in Fig. 3.

For a stationary observer, since the contribution of dominant quasi-normal modes is much larger than that of the other modes, the observed waveform equals approximately the dominant quasi-normal mode,

$$\Phi \sim C \cdot e^{-i\omega t} = C \cdot e^{-i \cdot 2M\omega \bar{t}}, \quad (25)$$

where C is the quasi-normal excitation coefficient corresponding to the dominant mode ω . Then we give the difference of \bar{t} between two adjacent peaks in the damping oscillation region on the $\log |\Phi| - \bar{t}$ plot,

$$\Delta \bar{t} = \frac{\pi}{2M\omega_{\text{R}}}, \quad (26)$$

and the ordinate difference between two adjacent peaks,

$$\Delta \log |\Phi| = \frac{\pi\omega_{\text{I}}}{\omega_{\text{R}}}. \quad (27)$$

Table 2: This table shows the types of waveforms and quasi-normal modes under the scalar field perturbation with $l = 2$, where the case of $\bar{a} \leq 1$ corresponds to Schwarzschild black holes, and the case of $1.000001 \leq \bar{a} \leq 1.001$ corresponds to Schwarzschild traversable wormholes with obvious echoes but the case of $1.1 \leq \bar{a} \leq 10.0$ corresponds to Schwarzschild traversable wormholes only with damping oscillations.

\bar{a}	$2M\omega$ (waveforms/QNMs)	\bar{a}	$2M\omega$ (waveforms/QNMs)
≤ 1 (black holes)	0.967508 - 0.193780 i	1.7	0.881462 - 0.194273 i
1.000001	Echo	1.8	0.847602 - 0.198093 i
1.00001	Echo	1.9	0.814952 - 0.199712 i
1.0001	Echo	2.0	0.783926 - 0.199760 i
1.001	Echo	3.0	0.556853 - 0.171306 i
1.01	0.916457 - 0.012704 i (Weak echo)	4.0	0.428506 - 0.141430 i
1.1	0.952315 - 0.035264 i	5.0	0.347028 - 0.118807 i
1.2	1.007350 - 0.090619 i	6.0	0.291499 - 0.103299 i
1.3	1.004790 - 0.131173 i	7.0	0.250827 - 0.090494 i
1.4	0.981648 - 0.158289 i	8.0	0.218958 - 0.079519 i
1.5	0.950439 - 0.176095 i	9.0	0.193980 - 0.072122 i
1.6	0.916186 - 0.187382 i	10.0	0.184465 - 0.069729 i

As a result, we obtain the slope of the line connecting two adjacent peaks,

$$\bar{k} = \frac{\Delta \log |\Phi|}{\Delta \bar{t}} = 2M\omega_{\text{I}}. \quad (28)$$

By calculating the quasi-normal modes with the Prony method under different values of \bar{a} , we give the plot of $2M\omega_{\text{R}}$ with respect to \bar{a} and the plot of $2M\omega_{\text{I}}$ with respect to \bar{a} in Fig. (4(a)) and Fig. 4(b), respectively, where the dots represent relevant data in Table 2. As depicted in Fig. 4, $2M\omega_{\text{R}}$ and $2M\omega_{\text{I}}$ are constants for Schwarzschild black holes, but vary with \bar{a} for Schwarzschild traversable wormholes. Therefore, $\Delta \bar{t}$, \bar{k} and $\Delta \log |\Phi|$ remain unchanged for Schwarzschild black holes, but vary with \bar{a} for Schwarzschild traversable wormholes in the $\log |\Phi| - \bar{t}$ plot. By comparing the differences in $\Delta \bar{t}$, \bar{k} , and $\Delta \log |\Phi|$ between these two types of spacetime, we are able to distinguish Schwarzschild black holes from Schwarzschild traversable wormholes. To this end, we need the physical time t and the other quantities with dimension, such as k . According to the relationship Eq. (12) between the dimensionless time and the physical time, the physical time interval and the corresponding slope between two adjacent peaks take the forms,

$$\Delta t = 2M\Delta \bar{t}, \quad k = \frac{\bar{k}}{2M}. \quad (29)$$

We can see that the two quantities change with M for Schwarzschild black holes. Since we do not have the data on the mass parameter M , we cannot distinguish Schwarzschild black holes from Schwarzschild traversable wormholes by using Δt and k . However, the quantity $\Delta \log |\Phi|$ remains unchanged with M for Schwarzschild black holes, but varies with \bar{a} for Schwarzschild traversable wormholes. Therefore, we can use the value of $\Delta \log |\Phi|$ to distinguish these two spacetimes. According to the quasi-normal mode of Schwarzschild black holes, $2M\omega = 0.967508 - 0.193780i$, see the second row in Table 2, and

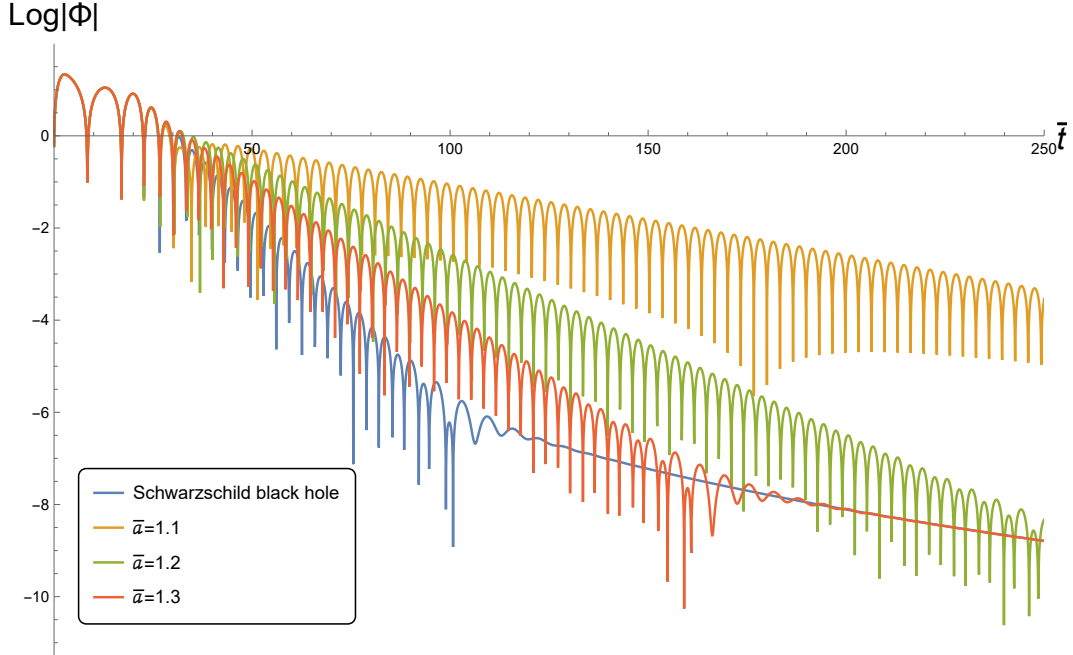


Figure 3: This figure shows the damping oscillation waveforms under the scalar field perturbation with $l = 2$ for different values of the parameter \bar{a} , where the blue curve corresponds to Schwarzschild black holes as a comparison, while the orange, green, and red curves correspond Schwarzschild traversable wormholes in the cases of $\bar{a} = 1.1, 1.2, 1.3$, respectively.

Eq. (27), we obtain

$$\Delta \log |\Phi| = \frac{-0.193780}{0.967508} \pi \approx -0.629223. \quad (30)$$

If the difference of $\log |\Phi|$ between adjacent peaks in damping oscillations deviates significantly from Eq. (30), we can infer that the spacetime prefers not to be Schwarzschild black holes but rather to be Schwarzschild traversable wormholes.

4.3 Scenario for fixing parameters

In the experimental observations [20, 21], the waveform data are depicted by a $\Phi - t$ plot, and then the corresponding $\log |\Phi| - t$ plot can be obtained by data processing. In the $\log |\Phi| - t$ plot, we can extract two parameters: the time interval between adjacent peaks, Δt , and the difference of $\log |\Phi|$ between adjacent peaks, $\Delta \log |\Phi|$. With these two parameters, we can determine the parameters M and a for Schwarzschild traversable wormholes by following the three steps:

- By fixing the value of $\Delta \log |\Phi|$, we give the value of \bar{a} in Fig. 5 that is a theoretical plot we draw up in accordance with Eq. (27) and Fig. (4);
- By using the value of \bar{a} , we get $2M\omega_R$ in Fig. 4;
- By using Eqs. (26) and (29), together with the value of Δt , we obtain the mass parameter,

$$M = \frac{\Delta t}{2\Delta \bar{t}} = \frac{(2M\omega_R)\Delta t}{2\pi}, \quad (31)$$

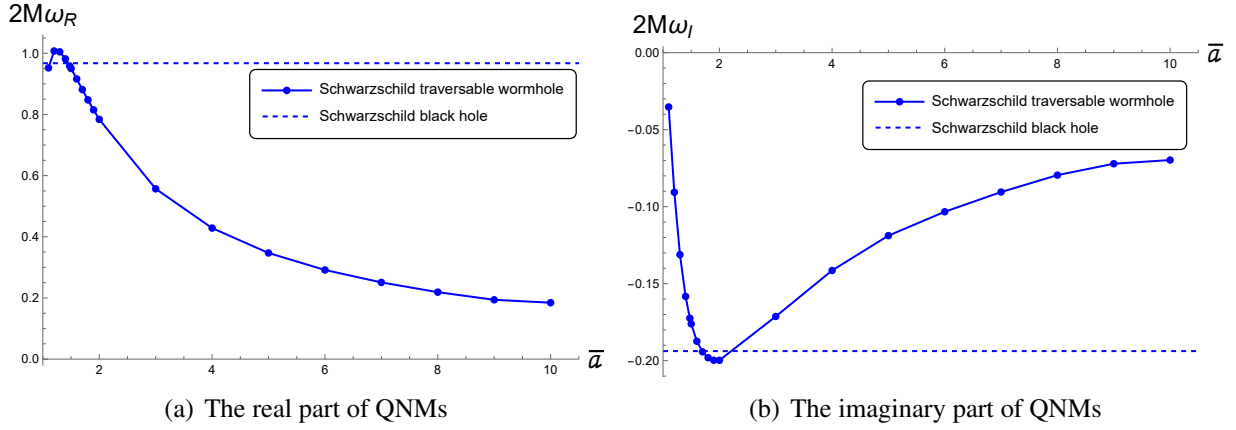


Figure 4: The two plots show how the real and imaginary parts of quasi-normal modes vary with the parameter \bar{a} under the scalar field perturbation with $l = 2$. The dotted lines represent the case of Schwarzschild black holes, while the solid curves represent the case of Schwarzschild traversable wormholes, where the dots represent relevant data given by Table 2.

and then the parameter a by combining M and \bar{a} as follows,

$$a = 2M\bar{a}. \quad (32)$$

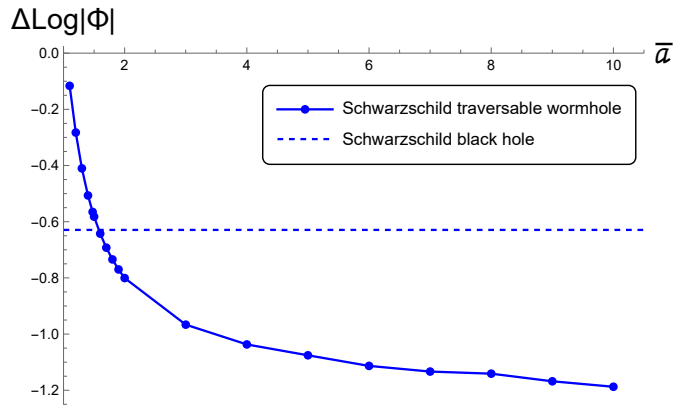


Figure 5: This figure shows how the difference of $\log |\Phi|$ between adjacent peaks, $\Delta \log |\Phi|$, varies with the parameter \bar{a} under the scalar field perturbation with $l = 2$. The dotted line represents the case of Schwarzschild black holes, while the solid curve represents the case of Schwarzschild traversable wormholes, where the dots represent relevant data given by Table 2.

5 Electromagnetic field perturbation

The waveform types under the electromagnetic field perturbation are similar to those under the scalar field perturbation, where the reason is that the effective potential of the electromagnetic field perturbation has the similar shape to that of the scalar field perturbation. For a more intuitive comparison, we present

the effective potentials under various field perturbations in Fig. 6 by using Eqs. (16)-(19), where $l = 2$ and $\bar{a} = 1.000001$ are set. However, the peak values of effective potentials are different for different field perturbations, which will influence the quasi-normal modes and the peak values of echoes.

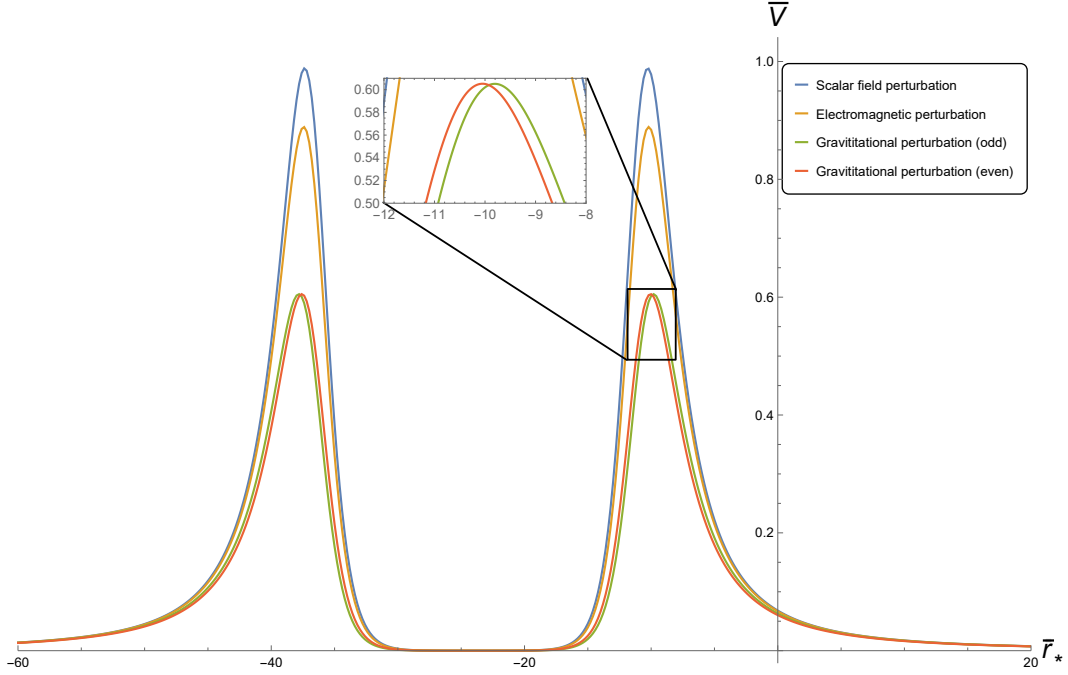


Figure 6: The figure shows the effective potentials under various field perturbations, where $l = 2$ and $\bar{a} = 1.000001$ are set. The blue, orange, green and red curves correspond the scalar field, electromagnetic field, odd parity gravitational field, and even parity gravitational field perturbations, respectively.

5.1 Echo waveform

The waveform of electromagnetic field perturbations contains an echo when $\bar{a} > 1$ and $\bar{a} - 1 \ll 1$. Within this range, we use the finite difference method to calculate the waveform and extract the occurrence time and peak values of echoes. In Fig. 7, we show the waveform under the electromagnetic field perturbation when $\bar{a} = 1.000001$. In Table 3, we list the time that the first three echoes occur and the peak values of echoes under different values of parameter \bar{a} .

Table 3: The time that the first three echoes occur and the peaks of these echoes under different values of the parameter \bar{a} for electromagnetic field perturbations.

\bar{a}	Echo 1 (T)	Echo 1 (P)	Echo 2 (T)	Echo 2 (P)	Echo 3 (T)	Echo 3 (P)
1.000001	86.4	0.620130	151.65	0.249708	209.75	0.150211
1.00001	77.2	0.620059	133.2	0.249948	182.05	0.154092
1.0001	67.95	0.620921	114.75	0.251282	161.70	0.145785
1.001	58.75	0.623614	99.80	0.235031	141.30	0.166783

By comparing Table 1 with Table 3, we analyze the similarities and differences between waveforms of scalar field perturbations and electromagnetic field perturbations. It is similar to the case of scalar field

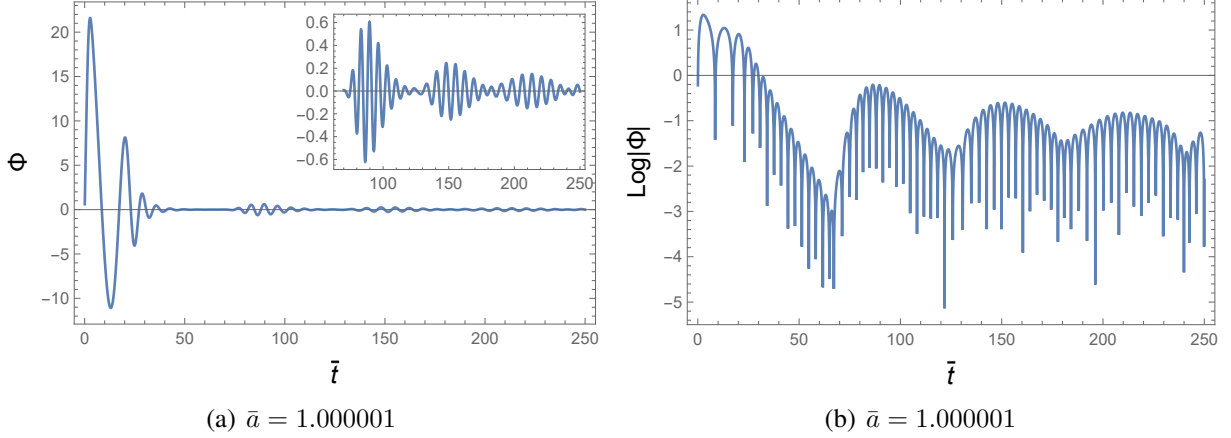


Figure 7: The echo waveform around Schwarzschild traversable wormholes for $\bar{a} = 1.000001$ under the electromagnetic field perturbation with $l = 2$. The left diagram shows how the wave function Φ varies with the time \bar{t} , and the right one shows how the function $\log |\Phi|$ varies with the time \bar{t} .

perturbations that the variation of parameter \bar{a} has little influence on the peak value of every order echo. Moreover, the peak value of each order echo for a fixed \bar{a} under the electromagnetic field perturbation is higher than that of the same order echo under the scalar field perturbation. The reason is that the peak value of effective potentials in the electromagnetic field perturbation is lower than that in the scalar field perturbation, which indicates that the former potential barrier has a weaker scattering effect on waves than the latter one, resulting in a higher echo peak for the former.

5.2 Damping oscillation

When \bar{a} is increasing, the waveform of electromagnetic field perturbations changes from echoes to damping oscillations, which is similar to that of scalar field perturbations. In Table 4, we show the quasi-normal modes computed by the Prony method for different values of \bar{a} . Comparing Table 4 with Table 2, we observe that both the real parts and absolute values of imaginary parts under the electromagnetic field perturbation are smaller than those under the scalar field perturbation for a fixed \bar{a} . This behavior indicates that the oscillation period of electromagnetic field perturbations is longer than that of scalar field perturbations, and that the modes are more stable under electromagnetic field perturbations. The reason is that the peak value of effective potentials is smaller in the electromagnetic field perturbation, which decreases the suppression effect of potential barriers on waveforms.

Next, we present by numerical calculations the plots of $2M\omega_R$ and $2M\omega_I$ with respect to \bar{a} in Fig. 8(a) and Fig. 8(b), respectively, where the dots denote the relevant data given in Table 4. By using Eq. (27) and Fig. 8, we obtain the plot of $\Delta \log |\Phi|$ with respect to \bar{a} in Fig. 9. According to the quasi-normal mode of Schwarzschild black holes, $2M\omega = 0.915464 - 0.190100i$, see the second row in Table 4, and Eq. (27), we figure out

$$\Delta \log |\Phi| = \frac{-0.190100}{0.915464} \pi \approx -0.652365. \quad (33)$$

If the difference of $\log |\Phi|$ between adjacent peaks in the damping oscillation of electromagnetic field

Table 4: This table shows the waveform types and quasi-normal modes under the electromagnetic field perturbation with $l = 2$, where the case of $\bar{a} \leq 1$ corresponds to Schwarzschild black holes, and the case of $1.000001 \leq \bar{a} \leq 1.001$ corresponds to Schwarzschild traversable wormholes with obvious echoes but the case of $1.1 \leq \bar{a} \leq 10.0$ corresponds to Schwarzschild traversable wormholes only with damping oscillations.

\bar{a}	waveform/QNM ($2M\omega$)	\bar{a}	waveform/QNM ($2M\omega$)
≤ 1	0.915464 - 0.190100 i	1.7	0.844303 - 0.185849 i
1.000001	Echo	1.8	0.813333 - 0.189897 i
1.00001	Echo	1.9	0.783507 - 0.191816 i
1.0001	Echo	2.0	0.754935 - 0.192228 i
1.001	Echo	3.0	0.542394 - 0.166944 i
1.01	0.877937 - 0.014752 i (Weak echo)	4.0	0.419618 - 0.138658 i
1.1	0.900571 - 0.034332 i	5.0	0.342186 - 0.117842 i
1.2	0.953902 - 0.086300 i	6.0	0.287567 - 0.102703 i
1.3	0.953680 - 0.124633 i	7.0	0.247981 - 0.089702 i
1.4	0.933921 - 0.150537 i	8.0	0.213115 - 0.075908 i
1.5	0.906326 - 0.167754 i	9.0	0.191102 - 0.068795 i
1.6	0.875648 - 0.178906 i	10.0	0.172544 - 0.057280 i

perturbations deviates significantly from Eq. (33), we can infer that the spacetime prefers Schwarzschild traversable wormholes but not Schwarzschild black holes. Moreover, using the plot of $\log |\Phi| - t$, we can also determine the parameters M and a in terms of Figs. 8(a) and 9 together with the scenario for fixing parameters introduced in Sec. 4.3.

6 Gravitational field perturbation

6.1 Echo waveform

The echo waveform under the gravitational field perturbation also appears in the range of $\bar{a} > 1$ and $\bar{a} - 1 \ll 1$. In Tables 5 and 6, we present the time that the first three echoes occur and the peak values of echoes under the odd and even parity perturbations, respectively. By comparing these two tables, we find that the occurrence time for the echoes under the even parity perturbation is always earlier than that under the odd parity perturbation. For the first echo with any value of \bar{a} , there is a fixed occurrence time interval $\Delta T = 0.50$ with a numerical error of ± 0.05 between the even and odd parity perturbations. This fixed time interval becomes $3\Delta T$ for the second echo, and $5\Delta T$ for the third echo. As shown in Fig. 6, the potential barrier of the even parity perturbation is closer to the throat of wormholes, resulting in a smaller distance between the double potential barriers. Therefore, the propagation time of waves between the double potential barriers is shorter under even parity perturbations, leading to earlier and more frequent echoes.

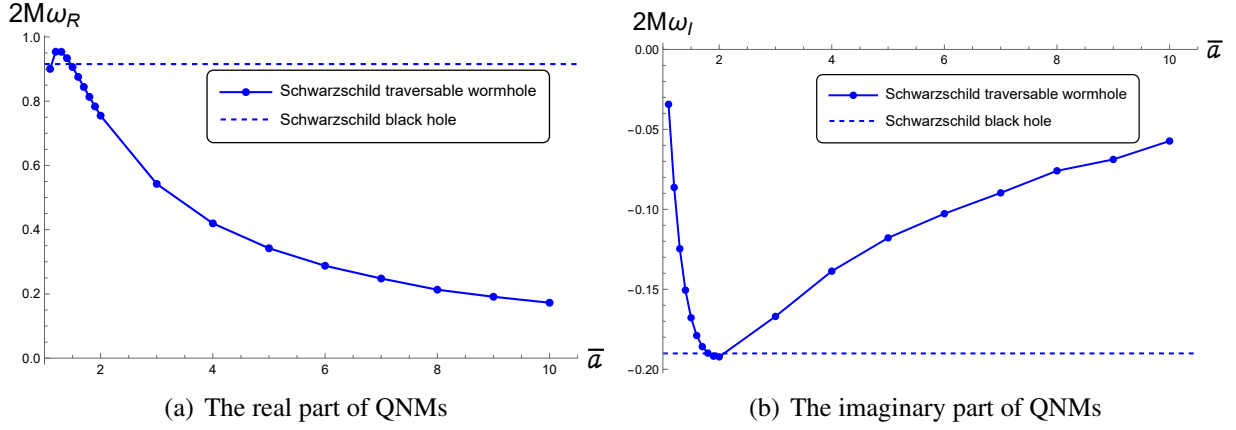


Figure 8: The figure shows how the real and imaginary parts of quasi-normal modes vary with the parameter \bar{a} under the electromagnetic field perturbation with $l = 2$. The dotted lines represent the case of Schwarzschild black holes, while the solid curves represent the case of Schwarzschild traversable wormholes, where the dots denote the relevant data given in Table 4.

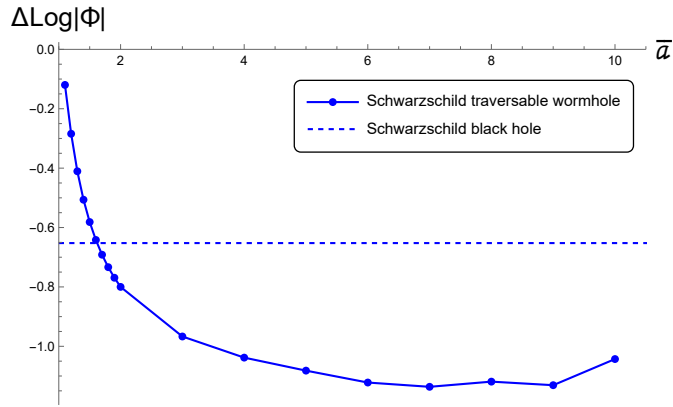


Figure 9: This figure shows how the difference of $\log |\Phi|$ between adjacent peaks, $\Delta \log |\Phi|$, varies with the parameter \bar{a} under the electromagnetic field perturbation with $l = 2$. The dotted line represents the case of Schwarzschild black holes, while the solid curve represents the case of Schwarzschild traversable wormholes, where the dots denote the relevant data given in Table 4.

Table 5: The time that the first three echoes occur and the peaks of these echoes under different values of the parameter \bar{a} for odd parity gravitational field perturbations.

\bar{a}	Echo 1 (T)	Echo 1 (P)	Echo 2 (T)	Echo 2 (P)	Echo 3 (T)	Echo 3 (P)
1.000001	87.55	0.836331	153.80	0.332283	215.80	0.200644
1.00001	78.35	0.836018	135.40	0.330864	188.10	0.202523
1.0001	69.10	0.834329	116.95	0.334547	155.85	0.224136
1.001	59.90	0.829503	94.05	0.352147	128.40	0.251196

Table 6: The time that the first three echoes occur and the peaks of these echoes under different values of the parameter \bar{a} for even parity gravitational field perturbations.

\bar{a}	Echo 1 (T)	Echo 1 (P)	Echo 2 (T)	Echo 2 (P)	Echo 3 (T)	Echo 3 (P)
1.000001	87.05	0.832113	152.30	0.330936	213.25	0.200990
1.00001	77.80	0.831670	133.85	0.330347	185.65	0.204183
1.0001	68.60	0.830169	115.40	0.338658	153.00	0.225835
1.001	59.35	0.829464	92.65	0.375115	126.15	0.251956

6.2 Damping oscillation and isospectrality

For Schwarzschild black holes, the odd and even parity perturbations have [28] the isospectrality, meaning that the quasi-normal modes are exactly the same, i.e., they are independent of parities. For Schwarzschild traversable wormholes, however, the isospectrality is invalid in the quasi-normal modes of damping oscillation waveforms. In Fig. 10, we present the damping oscillations in the black hole and wormhole spacetimes under odd and even parity gravitational field perturbations with $l = 2$. In Schwarzschild black holes, the waveform of the odd parity perturbation coincides with that of the even parity perturbation, confirming the isospectrality. In Schwarzschild traversable wormholes, however, the waveform of the odd parity perturbation is clearly distinguishable from that of the even parity perturbation. More specifically, we show the data of quasi-normal modes for odd and even parity perturbations in Tables 7 and 8, respectively. By comparing the data in the two tables, we find that the isospectrality is indeed invalid in Schwarzschild traversable wormholes.

Now we turn to the reason for the breaking of isospectrality. By analyzing the asymptotic behavior of the effective potentials described by Eqs. (10) and (11) near the boundaries, we find that the even parity effective potential exhibits an asymptotic behavior consistent with that of the odd parity effective potential in Schwarzschild black holes when the former is shifted by a distance $\Delta\bar{r}_* = 0.25$ along the \bar{r}_* -coordinate direction. In Schwarzschild traversable wormholes, however, the throat introduces a mirror symmetry, thereby altering the asymptotic behavior of effective potentials near the boundaries and disrupting the aforementioned translational symmetry between odd and even parity effective potentials. Since the quasi-normal modes are closely related to the asymptotic behavior near the boundaries, the usual isospectrality that exists in Schwarzschild black holes no longer holds in Schwarzschild traversable wormholes.

Nevertheless, we find an alternative isospectrality in Schwarzschild traversable wormholes under odd and even parity gravitational field perturbations. Here we consider two different wormholes, ‘‘O’’ and

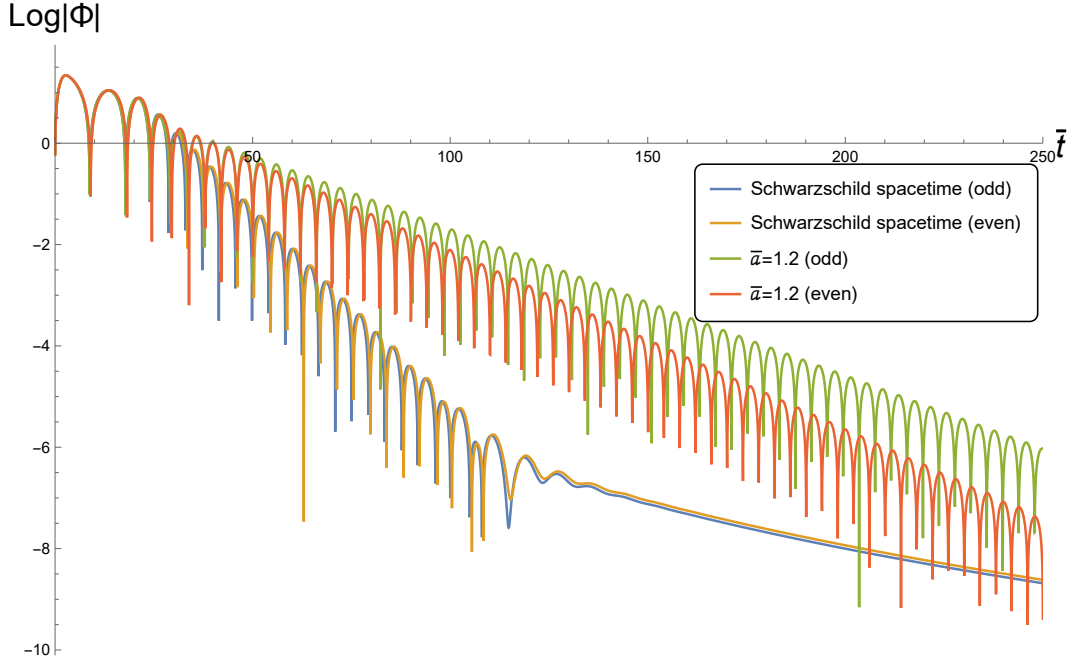


Figure 10: This figure shows the damping oscillations under the gravitational field perturbation, where the blue and orange curves represent the odd and even parity perturbations in Schwarzschild black holes, and the green and red curves represent the odd and even parity perturbations in Schwarzschild traversable wormholes with $\bar{a} = 1.2$.

Table 7: This table shows the waveform types and quasi-normal modes under the odd parity gravitational field perturbation with $l = 2$, where the case of $\bar{a} \leq 1$ corresponds to Schwarzschild black holes, the case of $1.000001 \leq \bar{a} \leq 1.001$ corresponds to Schwarzschild traversable wormholes with obvious echoes, and the case of $1.1 \leq \bar{a} \leq 10.0$ corresponds to Schwarzschild traversable wormholes only with damping oscillations.

\bar{a}	waveform/QNM ($2M\omega$)	\bar{a}	waveform/QNM ($2M\omega$)
≤ 1	0.747450 - 0.178107 i	1.7	0.727195 - 0.155295 i
1.000001	Echo	1.8	0.706166 - 0.160560 i
1.00001	Echo	1.9	0.685190 - 0.163871 i
1.0001	Echo	2.0	0.664565 - 0.165691 i
1.001	Echo	3.0	0.498185 - 0.152153 i
1.01	0.741595 - 0.020092 i (Weak echo)	4.0	0.394052 - 0.129780 i
1.1	0.725765 - 0.027264 i	5.0	0.324647 - 0.111235 i
1.2	0.777911 - 0.066573 i	6.0	0.275629 - 0.096729 i
1.3	0.787784 - 0.097540 i	7.0	0.239082 - 0.085672 i
1.4	0.780846 - 0.120006 i	8.0	0.211504 - 0.076267 i
1.5	0.766049 - 0.136103 i	9.0	0.189583 - 0.069135 i
1.6	0.747529 - 0.147468 i	10.0	0.171488 - 0.062760 i

“E”, where their dimensionless parameters are denoted by $\bar{a}_{(o)}$ and $\bar{a}_{(e)}$, respectively. The two wormholes have no interactions with each other. According to Eq. (15), their throats are located at $\bar{a}_{(o)} + \ln(\bar{a}_{(o)} - 1)$

Table 8: This table shows the waveform types and quasi-normal modes under the even parity gravitational field perturbation with $l = 2$, where the case of $\bar{a} \leq 1$ corresponds to Schwarzschild black holes, the case of $1.000001 \leq \bar{a} \leq 1.001$ corresponds to Schwarzschild traversable wormholes with obvious echoes, and the case of $1.1 \leq \bar{a} \leq 10.0$ corresponds to Schwarzschild traversable wormholes only with damping oscillations.

\bar{a}	waveform/QNM ($2M\omega$)	\bar{a}	waveform/QNM ($2M\omega$)
≤ 1	0.747432 - 0.178120 i	1.7	0.705028 - 0.160865 i
1.000001	Echo	1.8	0.682381 - 0.164247 i
1.00001	Echo	1.9	0.660390 - 0.166128 i
1.0001	Echo	2.0	0.639233 - 0.166596 i
1.001	Echo	3.0	0.477372 - 0.148201 i
1.01	0.763379 - 0.027204 i (Weak echo)	4.0	0.378346 - 0.125969 i
1.1	0.745977 - 0.037487 i	5.0	0.313210 - 0.108521 i
1.2	0.785279 - 0.081459 i	6.0	0.266550 - 0.093576 i
1.3	0.784918 - 0.112186 i	7.0	0.233528 - 0.080293 i
1.4	0.770441 - 0.132667 i	8.0	0.205944 - 0.076657 i
1.5	0.750292 - 0.146268 i	9.0	0.183167 - 0.066145 i
1.6	0.727983 - 0.155230 i	10.0	0.159704 - 0.060145 i

and $\bar{a}_{(e)} + \ln(\bar{a}_{(e)} - 1)$ in the \bar{r}_* coordinate, respectively. If there is a translational symmetry between these two throats,

$$\bar{a}_{(e)} + \ln(\bar{a}_{(e)} - 1) + \Delta\bar{r}_* = \bar{a}_{(o)} + \ln(\bar{a}_{(o)} - 1), \quad (34)$$

we can shift the even parity effective potential of the ‘‘E’’ wormhole by a distance $\Delta\bar{r}_* = 0.25$ along the \bar{r}_* -coordinate direction and find that it exhibits an asymptotic behavior consistent with that of the odd parity effective potential of the ‘‘O’’ wormhole by analyzing the asymptotic behavior of the effective potentials depicted by Eqs. (18) and (19) at the boundaries. This relationship is same as that between the odd and even parity effective potentials in Schwarzschild black holes. Therefore, we further analyze whether there is the isospectrality between the quasi-normal modes of the ‘‘O’’ and ‘‘E’’ wormholes. Taking the values of \bar{a} appeared in Table 7 as $\bar{a}_{(o)}$, we obtain $\bar{a}_{(e)}$ by using Eq. (34) and calculate the quasi-normal modes of the ‘‘E’’ wormhole under the even parity perturbation. If defining the relative difference between two data as

$$D = \frac{|\text{datum1} - \text{datum2}|}{|\text{datum1}|}, \quad (35)$$

we give the corresponding results in Table. 9, where the two items stand for the relative difference between the real parts and between the imaginary parts of QNMs, respectively, in each parenthesis of the fifth column. We notice that these relative differences are almost less than 0.100%. After comparing these data, we can draw a conclusion: If the translational symmetry exists, see Eq. (34), the ‘‘O’’ wormhole under the odd parity perturbation has the same quasi-normal modes as the ‘‘E’’ wormhole under the even parity perturbation does, that is, an unusual isospectrality is established between the two special wormholes.

Finally, we present the plots of $2M\omega_R$ and $2M\omega_I$ varying with \bar{a} in Figs. (11(a)) and 11(b), respectively, where the blue and orange dots depend on the relevant data in Table 7 and Table 8, re-

Table 9: This table shows the quasi-normal modes of the wormhole with $\bar{a}_{(e)}$ under the even parity gravitational field perturbation and those of the wormhole with $\bar{a}_{(o)}$ under the odd parity gravitational field perturbation, where $\bar{a}_{(e)}$ and $\bar{a}_{(o)}$ that appear in the same row satisfy the relationship, Eq. (34).

$\bar{a}_{(o)}$	QNM ($2M\omega$)	$\bar{a}_{(e)}$	QNM ($2M\omega$)	the relative difference
1.1	0.725765 - 0.027264 i	1.079	0.725670 - 0.027187 i	(0.013%, 0.280%)
1.2	0.777911 - 0.066573 i	1.162	0.778005 - 0.066442 i	(0.012%, 0.197%)
1.3	0.787784 - 0.097540 i	1.246	0.787697 - 0.097444 i	(0.011%, 0.098%)
1.4	0.780846 - 0.120006 i	1.333	0.781029 - 0.119827 i	(0.023%, 0.149%)
1.5	0.766049 - 0.136079 i	1.421	0.766445 - 0.136038 i	(0.052%, 0.030%)
1.6	0.747529 - 0.147468 i	1.511	0.747935 - 0.147447 i	(0.054%, 0.014%)
1.7	0.727195 - 0.155295 i	1.602	0.727593 - 0.155347 i	(0.055%, 0.033%)
1.8	0.706166 - 0.160560 i	1.693	0.706565 - 0.160569 i	(0.056%, 0.006%)
1.9	0.685190 - 0.163871 i	1.786	0.685534 - 0.163854 i	(0.050%, 0.010%)
2.0	0.664565 - 0.165691 i	1.879	0.664721 - 0.165757 i	(0.023%, 0.040%)
3.0	0.498499 - 0.152337 i	2.836	0.498294 - 0.152188 i	(0.041%, 0.098%)
4.0	0.393727 - 0.129644 i	3.814	0.393819 - 0.129720 i	(0.023%, 0.059%)
5.0	0.324484 - 0.111145 i	4.801	0.324488 - 0.111174 i	(0.001%, 0.026%)
6.0	0.275629 - 0.096729 i	5.792	0.275611 - 0.096722 i	(0.006%, 0.007%)
7.0	0.239384 - 0.085369 i	6.786	0.239386 - 0.085322 i	(0.001%, 0.055%)
8.0	0.211546 - 0.076363 i	7.782	0.211570 - 0.076350 i	(0.011%, 0.017%)
9.0	0.189428 - 0.069051 i	8.778	0.189492 - 0.068995 i	(0.034%, 0.081%)
10.0	0.171543 - 0.062854 i	9.775	0.171527 - 0.062889 i	(0.009%, 0.056%)

spectively. According to Fig. 11 and Eq. (27), we plot $\Delta \log |\Phi|$ with respect to \bar{a} in Fig. 12. For Schwarzschild black holes, we compute $\Delta \log |\Phi|$ by using the quasi-normal mode of odd parity perturbations, $2M\omega = 0.747450 - 0.178107i$,

$$\Delta \log |\Phi| = \frac{-0.178107}{0.747450} \pi \approx -0.748598, \quad (36)$$

and similarly give the corresponding $\Delta \log |\Phi|$ by using the quasi-normal mode of even parity perturbations, $2M\omega = 0.747432 - 0.178120i$,

$$\Delta \log |\Phi| = \frac{-0.178120}{0.747432} \pi \approx -0.748671. \quad (37)$$

Their relative difference is 0.010%, which shows that $\Delta \log |\Phi|$ is the same for both the odd and even parity perturbations. However, $\Delta \log |\Phi|$ differs owing to parities in Schwarzschild traversable wormholes as depicted by Fig. 12. Therefore, we may distinguish a Schwarzschild traversable wormhole from a Schwarzschild black hole by measuring such a quantity. In addition, we can determine the parameters M and a in terms of Fig. 10, the plot of $\log |\Phi| - t$ by observations, together with Figs. 11 and 12, when we follow the scenario introduced in Sec. 4.3. In particular, we can determine the range of parameters more accurately by jointly calculating various field perturbations, such as the scalar field, the electromagnetic field, and the gravitational field perturbations.

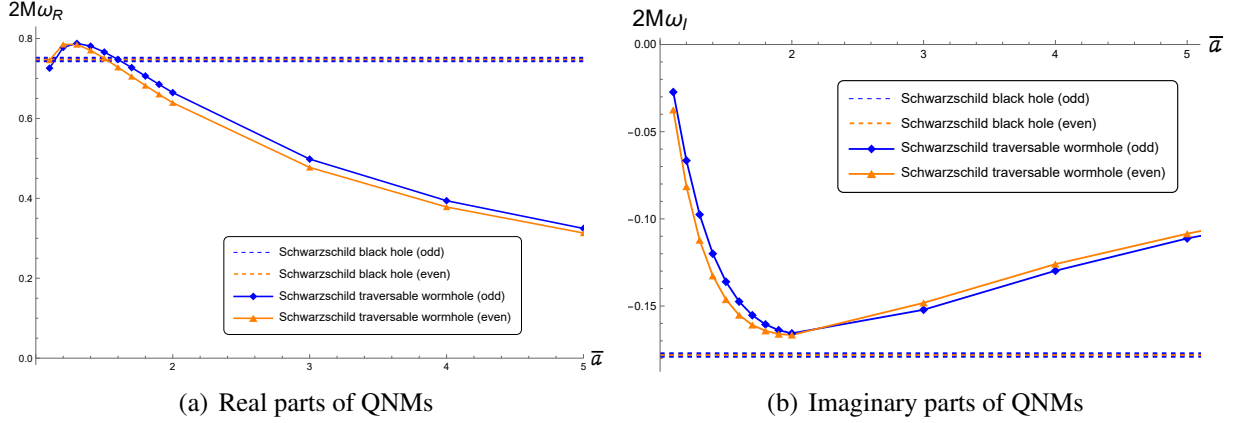


Figure 11: The figure shows how the real and imaginary parts of quasi-normal modes vary with the parameter \bar{a} under the gravitational field perturbation with $l = 2$. The blue and orange dotted lines represent the case of Schwarzschild black holes under the odd and even parity perturbations, respectively, while the blue and orange solid curves represent the case of Schwarzschild traversable wormholes under the odd and even parity perturbations, respectively, where the blue and orange dots depend on the relevant data in Table 7 and 8, respectively.

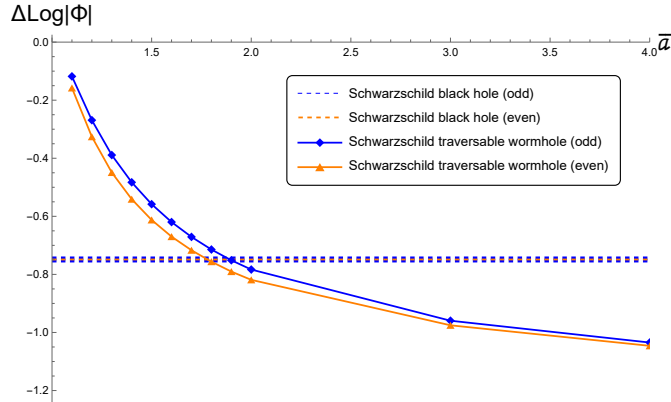


Figure 12: The figure shows how the difference value $\Delta \log |\Phi|$ between adjacent peaks varies with parameter \bar{a} under the gravitational perturbation with $l = 2$. The blue and orange dotted lines represent the case of Schwarzschild black holes under the odd and even parity perturbations, respectively, while the blue and orange solid curves represent the case of Schwarzschild traversable wormholes under the odd and even parity perturbations, respectively, where the blue and orange dots depend on the relevant data in Table 7 and 8, respectively.

7 Conclusion and discussion

We investigate the properties of Schwarzschild traversable wormholes and find their crucial factor — the position of throats, where such a model is primarily obtained by taking the “cut and paste” technique in the Schwarzschild spacetime. Moreover, we numerically calculate the waveform and quasi-normal modes of the scalar field perturbation, the electromagnetic perturbation, and the gravitational field perturbation for the model. By comparing the properties of Schwarzschild traversable wormholes with those of Schwarzschild black holes, we obtain the following unique features for the former:

- When a Schwarzschild wormhole has just transformed from a Schwarzschild black hole or is about to transform into the black hole, the perturbation waveform of all fields exhibits the echo waveform, which does not appear in a Schwarzschild black hole.
- In a damping oscillation waveform depicted by the plot of $\log |\Phi| - t$, the difference between adjacent peaks remains constant in a Schwarzschild black hole, but it varies with the change of $\frac{a}{2M}$ in a Schwarzschild traversable wormhole.
- In a Schwarzschild black hole, the even parity gravitational field perturbation gives rise to the same quas-normal modes as the odd parity gravitational field perturbation does, i.e., the isospectrality. However, such an isospectrality does not remain in a Schwarzschild traversable wormhole, i.e., the perturbation waveform and quasi-normal modes depend on parities.
- If two Schwarzschild traversable wormholes, “O” and “E” with the positions of throats $\bar{a}_{(o)}$ and $\bar{a}_{(e)}$, respectively, satisfy the translational symmetry, see Eq. (34), we find an unusual isospectrality, i.e., the quasi-normal modes of the wormhole “O” under the odd parity perturbation are same as those of the wormhole “E” under the even parity perturbation.

Based on these unique features, we summarize a scenario for estimating the parameters M and a from the plot of $\log |\Phi| - t$ and the numerical results of quasi-normal modes. Although it is only a theoretical concept at present, a Schwarzschild traversable wormhole is expected to be observed in future gravitational wave experiments through the above-mentioned features. If so, we shall gain more understanding and knowledge of the universe.

Acknowledgments

Y-GM would like to thank Emmanuele Battista, Stefan Fredenhagen, and Harold Steinacker for the warm hospitality during his stay at University of Vienna. This work was supported in part by the National Natural Science Foundation of China under Grant No. 12175108.

References

- [1] H Weyl. *Philosophy of mathematics and of natural sciences*, 1927. *English transl., Princeton University Press, Princeton, New Jersey*, 1949.

- [2] Albert Einstein and Nathan Rosen. The particle problem in the general theory of relativity. *Physical Review*, 48(1):73, 1935.
- [3] M. S. Morris and K. S. Thorne. Wormholes in space-time and their use for interstellar travel: A tool for teaching general relativity. *Am. J. Phys.*, 56:395–412, 1988. doi:10.1119/1.15620.
- [4] M. S. Morris, K. S. Thorne, and U. Yurtsever. Wormholes, Time Machines, and the Weak Energy Condition. *Phys. Rev. Lett.*, 61:1446–1449, 1988. doi:10.1103/PhysRevLett.61.1446.
- [5] Matt Visser. Traversable wormholes from surgically modified Schwarzschild space-times. *Nucl. Phys. B*, 328:203–212, 1989. arXiv:0809.0927, doi:10.1016/0550-3213(89)90100-4.
- [6] Matt Visser. Traversable wormholes: Some simple examples. *Phys. Rev. D*, 39:3182–3184, 1989. arXiv:0809.0907, doi:10.1103/PhysRevD.39.3182.
- [7] Matt Visser. Quantum wormholes. *Phys. Rev. D*, 43:402–409, 1991. doi:10.1103/PhysRevD.43.402.
- [8] G. P. Perry and Robert B. Mann. Traversable wormholes in (2+1)-dimensions. *Gen. Rel. Grav.*, 24:305–321, 1992. doi:10.1007/BF00760232.
- [9] Biplab Bhawal and Sayan Kar. Lorentzian wormholes in Einstein-Gauss-Bonnet theory. *Phys. Rev. D*, 46:2464–2468, 1992. doi:10.1103/PhysRevD.46.2464.
- [10] Martin G. Richarte and Claudio Simeone. Wormholes in Einstein-Born-Infeld theory. *Phys. Rev. D*, 80:104033, 2009. [Erratum: *Phys.Rev.D* 81, 109903 (2010)]. arXiv:2006.12272, doi:10.1103/PhysRevD.81.109903.
- [11] Ernesto F. Eiroa. Thin-shell wormholes with a generalized Chaplygin gas. *Phys. Rev. D*, 80:044033, 2009. arXiv:0907.2205, doi:10.1103/PhysRevD.80.044033.
- [12] Ernesto F. Eiroa, Martin G. Richarte, and Claudio Simeone. Thin-shell wormholes in Brans-Dicke gravity. *Phys. Lett. A*, 373:1–4, 2008. [Erratum: *Phys.Lett.* 373, 2399–2400 (2009)]. arXiv:0809.1623, doi:10.1016/j.physleta.2008.10.065.
- [13] Jose P. S. Lemos and Francisco S. N. Lobo. Plane symmetric thin-shell wormholes: Solutions and stability. *Phys. Rev. D*, 78:044030, 2008. arXiv:0806.4459, doi:10.1103/PhysRevD.78.044030.
- [14] F. Rahaman, M. Kalam, and S. Chakraborti. Thin shell wormhole in heterotic string theory. *Int. J. Mod. Phys. D*, 16:1669–1681, 2007. arXiv:gr-qc/0611134, doi:10.1142/S0218271807010924.
- [15] F. Rahaman, M. Kalam, and S. Chakraborty. Thin shell wormholes in higher dimensionaonal Einstein-Maxwell theory. *Gen. Rel. Grav.*, 38:1687–1695, 2006. arXiv:gr-qc/0607061, doi:10.1007/s10714-006-0325-y.

- [16] Marc Thibault, Claudio Simeone, and Ernesto F. Eiroa. Thin-shell wormholes in Einstein-Maxwell theory with a Gauss-Bonnet term. *Gen. Rel. Grav.*, 38:1593–1608, 2006. arXiv:gr-qc/0512029, doi:10.1007/s10714-006-0324-z.
- [17] Cecilia Bejarano and Ernesto F. Eiroa. Dilaton thin-shell wormholes supported by a generalized Chaplygin gas. *Phys. Rev. D*, 84:064043, 2011. arXiv:1106.6340, doi:10.1103/PhysRevD.84.064043.
- [18] Farook Rahaman, P. K. F. Kuhfittig, M. Kalam, A. A. Usmani, and Saibal Ray. A comparison of Hořava-Lifshitz gravity and Einstein gravity through thin-shell wormhole construction. *Class. Quant. Grav.*, 28:155021, 2011. arXiv:1011.3600, doi:10.1088/0264-9381/28/15/155021.
- [19] Renan B. Magalhães, Andreu Masó-Ferrando, Gonzalo J. Olmo, and Luís C. B. Crispino. Asymmetric wormholes in Palatini $f(R)$ gravity: Energy conditions, absorption, and quasibound states. *Phys. Rev. D*, 108(2):024063, 2023. arXiv:2303.03924, doi:10.1103/PhysRevD.108.024063.
- [20] B. P. Abbott et al. Observation of Gravitational Waves from a Binary Black Hole Merger. *Phys. Rev. Lett.*, 116(6):061102, 2016. arXiv:1602.03837, doi:10.1103/PhysRevLett.116.061102.
- [21] B. P. Abbott et al. GW170817: Observation of Gravitational Waves from a Binary Neutron Star Inspiral. *Phys. Rev. Lett.*, 119(16):161101, 2017. arXiv:1710.05832, doi:10.1103/PhysRevLett.119.161101.
- [22] R. Abbott et al. Observation of Gravitational Waves from Two Neutron Star–Black Hole Coalescences. *Astrophys. J. Lett.*, 915(1):L5, 2021. arXiv:2106.15163, doi:10.3847/2041-8213/ac082e.
- [23] Yiqian Chen, Peng Wang, Houwen Wu, and Haitang Yang. Observational appearance of a freely-falling star in an asymmetric thin-shell wormhole. *Eur. Phys. J. C*, 83(5):361, 2023. arXiv:2210.10948, doi:10.1140/epjc/s10052-023-11486-y.
- [24] Sen Guo, Guan-Ru Li, and En-Wei Liang. Optical appearance of a thin-shell wormhole with a Hayward profile. *Eur. Phys. J. C*, 83(7):663, 2023. arXiv:2210.03010, doi:10.1140/epjc/s10052-023-11842-y.
- [25] Shou-shan Bao, Shaoqi Hou, and Hong Zhang. Searching for wormholes with gravitational wave scattering. *Eur. Phys. J. C*, 83(2):127, 2023. arXiv:2201.05866, doi:10.1140/epjc/s10052-023-11281-9.
- [26] José T. Gálvez Gherzi, Andrei V. Frolov, and David A. Dobre. Echoes from the scattering of wavepackets on wormholes. *Class. Quant. Grav.*, 36(13):135006, 2019. arXiv:1901.06625, doi:10.1088/1361-6382/ab23c8.

- [27] S. Chandrasekhar and Steven L. Detweiler. The quasi-normal modes of the Schwarzschild black hole. *Proc. Roy. Soc. Lond. A*, 344:441–452, 1975. doi:10.1098/rspa.1975.0112.
- [28] Emanuele Berti, Vitor Cardoso, and Andrei O. Starinets. Quasinormal modes of black holes and black branes. *Class. Quant. Grav.*, 26:163001, 2009. arXiv:0905.2975, doi:10.1088/0264-9381/26/16/163001.
- [29] Vitor Cardoso, Edgardo Franzin, and Paolo Pani. Is the gravitational-wave ringdown a probe of the event horizon? *Phys. Rev. Lett.*, 116(17):171101, 2016. [Erratum: *Phys.Rev.Lett.* 117, 089902 (2016)]. arXiv:1602.07309, doi:10.1103/PhysRevLett.116.171101.
- [30] Hang Liu, Peng Liu, Yunqi Liu, Bin Wang, and Jian-Pin Wu. Echoes from phantom wormholes. *Phys. Rev. D*, 103(2):024006, 2021. arXiv:2007.09078, doi:10.1103/PhysRevD.103.024006.
- [31] Poulami Dutta Roy, S. Aneesh, and Sayan Kar. Revisiting a family of wormholes: geometry, matter, scalar quasinormal modes and echoes. *Eur. Phys. J. C*, 80(9):850, 2020. arXiv:1910.08746, doi:10.1140/epjc/s10052-020-8409-5.
- [32] Min-Yan Ou, Meng-Yun Lai, and Hyat Huang. Echoes from asymmetric wormholes and black bounce. *Eur. Phys. J. C*, 82(5):452, 2022. arXiv:2111.13890, doi:10.1140/epjc/s10052-022-10421-x.
- [33] Yi Yang, Dong Liu, Zhaoyi Xu, Yujia Xing, Shurui Wu, and Zheng-Wen Long. Echoes of novel black-bounce spacetimes. *Phys. Rev. D*, 104(10):104021, 2021. arXiv:2107.06554, doi:10.1103/PhysRevD.104.104021.
- [34] F. R. Klinkhamer. Defect Wormhole: A Traversable Wormhole Without Exotic Matter. *Acta Phys. Polon. B*, 54(5):5–A3, 2023. arXiv:2301.00724, doi:10.5506/APhysPolB.54.5-A3.
- [35] Alex Simpson and Matt Visser. Black-bounce to traversable wormhole. *JCAP*, 02:042, 2019. arXiv:1812.07114, doi:10.1088/1475-7516/2019/02/042.
- [36] Matt Visser. Lorentzian wormholes. from einstein to hawking. *Woodbury*, 1995.
- [37] R. A. Konoplya and A. Zhidenko. Quasinormal modes of black holes: From astrophysics to string theory. *Rev. Mod. Phys.*, 83:793–836, 2011. arXiv:1102.4014, doi:10.1103/RevModPhys.83.793.
- [38] Tullio Regge and John A Wheeler. Stability of a schwarzschild singularity. *Physical Review*, 108(4):1063, 1957.
- [39] Frank J Zerilli. Effective potential for even-parity regge-wheeler gravitational perturbation equations. *Physical Review Letters*, 24(13):737, 1970.

- [40] Emanuele Berti, Vitor Cardoso, Jose A. Gonzalez, and Ulrich Sperhake. Mining information from binary black hole mergers: A Comparison of estimation methods for complex exponentials in noise. *Phys. Rev. D*, 75:124017, 2007. arXiv:gr-qc/0701086, doi:10.1103/PhysRevD.75.124017.
- [41] Zhiying Zhu, Shao-Jun Zhang, C. E. Pellicer, Bin Wang, and Elcio Abdalla. Stability of Reissner-Nordström black hole in de Sitter background under charged scalar perturbation. *Phys. Rev. D*, 90(4):044042, 2014. [Addendum: Phys.Rev.D 90, 049904 (2014)]. arXiv:1405.4931, doi:10.1103/PhysRevD.90.044042.
- [42] N. Andersson. Excitation of Schwarzschild black hole quasinormal modes. *Phys. Rev. D*, 51:353–363, 1995. doi:10.1103/PhysRevD.51.353.